

1 **Mixing state and sources of submicron regional background aerosols in the**
2 **North Qinghai-Tibetan Plateau and the influence of biomass burning**

3

4 W.J. Li¹, S.R. Chen¹, Y.S. Xu², X. C. Guo^{1,2}, Y.L. Sun³, X.Y. Yang², Z.F. Wang³, X.D. Zhao⁴, J.M.
5 Chen¹, and W.X. Wang^{1,2}

6

7 ¹Environment Research Institute, Shandong University, 250100, Jinan, China,

8 ²Chinese Research Academy of Environmental Sciences, Beijing 100012, China

9 ³State Key Laboratory of Atmospheric Boundary Layer Physics and Atmospheric Chemistry, Institute
10 of Atmospheric Physics, Chinese Academy of Sciences, Beijing 100029, China

11 ⁴Qinghai Environmental Monitoring Center, Qinghai 810007, China.

12

13

14 Correspondence to liweijun@sdu.edu.cn (W.J. Li) and jmchen@sdu.edu.cn (J.M. Chen)

15 **Abstract:** Transmission electron microscopy (TEM) was employed to obtain morphology, size,
16 composition, and mixing state of background aerosols with diameter less than 1 μm in the North
17 Qinghai-Tibetan Plateau (QTP) during 15 September to 15 October, 2013. Individual aerosol
18 particles mainly contained secondary inorganic aerosols (SIA-sulfate and nitrate) and organics
19 during clean periods ($\text{PM}_{2.5}$ mass concentration less than $2.5 \mu\text{g}/\text{m}^3$). The presence of K-Na-Cl
20 associated with organics and an increase of soot particles suggest that an intense biomass burning
21 event caused the highest $\text{PM}_{2.5}$ concentrations ($> 30 \mu\text{g}/\text{m}^3$) during the study. A large number
22 fraction of the fly ash-containing particles (21.73%) suggests that coal combustion emissions in
23 the QTP significantly contributed to air pollutants at the medium pollution level ($\text{PM}_{2.5}$: 10-30
24 $\mu\text{g}/\text{m}^3$). We concluded that emissions from biomass burning and from coal combustion both
25 constantly contribute to anthropogenic particles in the QTP atmosphere. Based on size
26 distributions of individual particles in different pollution levels, we found that gas condensation on
27 existing particles is an important chemical process for the formation of SIA with organic coating.
28 TEM observations show that refractory aerosols (e.g., soot, fly ash, and visible organic particles)
29 likely adhere to the surface of SIA particles larger than 200 nm due to coagulation. Organic
30 coating and soot on surface of the aged particles likely influence their hygroscopic and optical
31 properties in the QTP, respectively. To our knowledge, this study reports the first microscopic
32 analysis of fine particles in the background QTP air.

33

34 **1. Introduction**

35 With an immense area (about 2,400,000 km²) and mean elevation of more than 4000 m above
36 sea level, the Tibetan Plateau (TP), called the “ridge of the world and third polar”, plays a key role
37 in Asian climatology, especially the formation of monsoons (Lau et al., 2006). Climate on the TP
38 has warmed 0.3 °C per decade over the past three decades, which is twice the rate of observed
39 global warming (Xu et al., 2009). Anthropogenic aerosols and their ice and cloud condensation
40 nuclei (CCN) directly or indirectly led to the brightening and dimming phenomenon before
41 and after the 1980s in the TP (You et al., 2010). However, light absorbing carbonaceous aerosol
42 particles (i.e., black carbon (BC) and brown carbon (BrC)) can warm the troposphere
43 (Ramanathan and Carmichael, 2008) and accelerate glacier retreat (Xu et al., 2009). Both the
44 radiative effects of aerosols and their role in cloud forming processes depend on their number, size,
45 chemical properties, and mixing state.

46 As a consequence, a better understanding of climate change can be achieved by characterizing
47 the TP aerosols. Quite a few aerosol measurements have been conducted in the TP. Ion
48 composition records from a shallow ice core (Zheng et al., 2010) and black soot in the Tibetan
49 glaciers (Xu et al., 2009) both showed that anthropogenic aerosols have increased significantly in
50 the most recent 50 years in the TP. Li et al. (2013a) obtained aerosol components such as 61%
51 mineral, 3% ammonium, 4% nitrate, 18% sulfate, 2% black carbon, and 12% organic matter in
52 PM_{2.5} at a concentration of 21.5 µg m⁻³ during summer of 2010 at Qinghai Lake (36°59'N,
53 99°54'E; 3200 m a.s.l.) in the northeastern part of the TP. Coal burning and biomass burning were
54 the major sources for anthropogenic aerosols. Xu et al. (2014) showed that the PM_{2.5} mass
55 concentration of 9.5 ± 5.4 µg m⁻³ during a year-long study at the Qilian Shan Station (39.50°N,
56 96.51°E; 4180 m a.s.l.), a remote site on the northeast edge of the Tibetan Plateau, and their water
57 soluble ionic species were dominated by SO₄²⁻ (39%), CO₃²⁻ (19%), Ca²⁺ (16%), NO₃⁻ (10%), and
58 NH₄⁺ (6%). The study suggests anthropogenic aerosol and natural mineral dust from the Gobi
59 desert together contribute to the particle loading in this remote air. Li et al. (2007) also found
60 anthropogenic ions from residential combustion emissions in precipitation samples at Nam Co
61 station of the central TP. In addition, long-range transport of pollutants from eastern and
62 northwestern China and northern India can contribute black carbon and other air pollutants to the

63 TP region (Cao et al., 2010;Wang et al., 2010;Engling et al., 2011;Kopacz et al., 2011;Lu et al.,
64 2012;Xu et al., 2013;Zhao et al., 2013;Cong et al., 2015;Duo et al., 2015). Although
65 anthropogenic sources make but a minor contribution to the background TP atmosphere, these
66 anthropogenic aerosols significantly enhanced aerosol optical properties (AOD) in the central and
67 northeastern TP in summer (Cong et al., 2009b;Che et al., 2011;Xia et al., 2011). Therefore, study
68 of the composition and sources of aerosol particles in the TP is necessary to understand their
69 effects on the optical, CCN or IN activity.

70 The TP has various geographic and natural environmental ecosystems such as mountains, lake
71 basins, deserts, forests, and grasslands. Previous sampling sites have included mountain forests,
72 lake basins , and urban areas in the TP (Li et al., 2007;Che et al., 2011;Engling et al., 2011;Li et al.,
73 2013a;Xu et al., 2014). Grassland is one of the largest geomorphology in the TP. There are only a
74 few herdsmen and farmers living in the vast grasslands of the norther TP. Air pollutants from
75 anthropogenic and natural sources can be easily transported over low bushes in the grasslands
76 under high wind speed in north TP (Figure S1). However, fine aerosols in the troposphere have not
77 been studied over the vast grassland in the northern TP. In this study, we collected samples at a
78 national station of background atmospheric monitoring (NSBAM) on the top of Moshidaban
79 mountain of Menyuan county in Qinghai province (37°35.370'N; 101°17.329'E; elevation: 3295
80 m), which is within the northern part of the Qinghai-Tibet Plateau (QTP) (Figure 1). The NSBAM
81 is 180 km north of Qinghai Lake (Li et al., 2013a) and 160 km from Waliguan station (Che et al.,
82 2011). Only a few herdsmen live in the grassland but many agricultural activities (e.g., growing
83 hulless barley and rape) mainly occur around Qinghai Lake and Menyuan County.

84 Although many atmospheric scientists have commented on the probable aerosol impacts on
85 climate and monsoon (Lau et al., 2006), atmospheric observations are still very limited because of
86 the unique geographic and natural environment, electric supply problems, high maintenance costs
87 for instruments, and lack of skilled operators. Because of the immensity of the TP, these previous
88 studies, quite scattered in diverse locations, are insufficient to adequately characterize the aerosols
89 throughout this vast region. In addition, the mixing state of individual particles has not been
90 examined, and only a few studies of particle types and soot have been conducted through electron
91 microscopy (Zhang et al., 2001a;Cong et al., 2009a). Understanding the mixing state of individual
92 particles sheds light on their source, ageing processes, optical, and hygroscopic properties (Posfai

93 and Buseck, 2010;Li et al., 2015). In the present study, high-resolution transmission electron
94 microscopy (TEM) is employed to study the mixing state and composition of individual
95 submicron particles with diameters $< 1 \mu\text{m}$. The pollution levels have been evaluated and
96 identified through continuous gaseous and particulate instruments at the sampling site. The
97 anthropogenic sources were further identified based on particle types in the QTP.

98

99 **2. Experimental methods**

100 **2.1 Aerosol sampling**

101 Aerosol particles were collected onto copper TEM grids coated with carbon film (carbon
102 type-B, 300-mesh copper, Tianld Co., China) by a two-stage impactor with a 1-mm-diameter jet
103 nozzle and a 0.5-mm-diameter jet nozzle and an air flow of 1.0 L min^{-1} . Both stages have a 50%
104 collection efficiency, the first at $0.80 \mu\text{m}$ and the second at $0.20 \mu\text{m}$, with an atmospheric pressure
105 of 69 kpa, a temperature of 283.5K, and an assumed particle density of 2 g/cm^3 . Sampling times
106 varied from 30 s to 15 min, depending on particle loading. After collection, each sample was
107 placed in a sealed, dry plastic tube and stored in a desiccator at $25 \text{ }^\circ\text{C}$ and $20 \pm 3\% \text{ RH}$ to minimize
108 exposure to ambient air and preserve it for analysis. Altogether, 70 individual samples were
109 collected at the NABAM with the elevation at 3295 m, of which we analyzed the fine particles
110 collected on only the second stage.

111 **2.2 Individual particle analysis**

112 21 aerosol particle samples collected on TEM grids were analyzed with a JEOL JEM-2100
113 TEM operated at 200 kV. The details about the aerosol collection were marked in Figure 2.
114 Elemental composition was determined semi-quantitatively by using an energy-dispersive X-ray
115 spectrometer (EDS) that can detect elements heavier than C. Cu was excluded from the analyses
116 because the TEM grids are made of Cu. The distribution of aerosol particles on TEM grids was not
117 uniform, with coarser particles occurring near the center and finer particles occurring on the
118 periphery. Therefore, to ensure that the analyzed particles were representative, five areas were
119 chosen from the center and periphery of the sampling spot on each grid. Every particle in the
120 selected area was analyzed. EDS spectra were collected for 15 s in order to minimize radiation
121 exposure and potential beam damage. To better understand the properties of internally mixed

122 aerosol particles, we also analyzed the composition of different components of individual particles,
 123 such as coatings, inclusions, and aggregations. The sampling was controlled to avoid coagulation
 124 on the substrate during sampling. The projected areas of individual particles were determined by
 125 the iTEM software (Olympus soft imaging solutions GmbH, Germany), the standard image
 126 analysis platform for electron microscopy. Altogether 4218 particles in these samples were
 127 measured for statistical analyses.

128 **2.3 Particle size measurement**

129 Atomic force microscopy (AFM) with a tapping mode analyzed aerosol particles under
 130 ambient conditions. AFM, a digital NanoscopeIIIa Instrument, can detect the
 131 three-dimensional morphology of particles. The AFM settings contain imaging forces
 132 between 1 and 1.5 nN, scanning rates between 0.5 and 0.8 Hz, and scanning range sizes at 10
 133 μm with a resolution of 512 pixels per length. After the AFM analysis, composition of the
 134 same particles was confirmed by TEM, with 194 fine aerosol particles analyzed by this
 135 method. The NanoScope analysis software can automatically obtain bearing area (A) and
 136 bearing volume (V) of each analyzed particle according to the following formula.

$$A = \pi r^2 = \pi \times \left(\frac{d}{2}\right)^2 = \frac{\pi d^2}{4} \rightarrow d = \sqrt{\frac{4A}{\pi}} \quad (1)$$

$$V = \frac{4}{3} \pi r^3 = \frac{4}{3} \times \frac{\pi D^3}{8} = \frac{\pi D^3}{6} \rightarrow D = \sqrt[3]{\frac{6V}{\pi}} \quad (2)$$

137 Where d is the equivalent circle diameter (ECD) and D is the equivalent volume diameter
 138 (EVD). By plotting the ECD against the EVD (Figure 3), we also obtain the relationship
 139 between them as $EVD=0.64ECD$. As a result, ECD (d) of individual aerosol particles
 140 measured from the iTEM software can be further converted into EVD (D) based on this
 141 relationship. In this study, we only considered fine aerosol particles with equivalent volume
 142 diameter smaller than 1 μm , where the correlation between the ECD and EVD is
 143 especially good (Figure 3).

144 **2.4 FLEXPART particle dispersion model**

145 Air mass history was determined using the Lagrangian particle dispersion model
 146 FLEXPART (version 9.02; (Stohl et al., 1998)). FLEXPART simulates the release of
 147 thousands of passive tracer air parcels at the specific location, advecting them backwards in

148 time, providing a representation of the spatial distribution of the air mass at an upwind time
149 referred to as a “retroplume”. FLEXPART was driven with 6 h meteorology data from NCEP
150 Climate Forecast System Version 2 (NCEP – CFSv2), including land cover, temperature,
151 relative humidity, and three- dimensional wind, in 37 levels with a resolution of $0.5^\circ \times 0.5^\circ$.
152 In this study, the modeling periods were 72h each simulations and it simulated 4 times each
153 day (beginning at 00:00, 06:00, 12:00, and 18:00, respectively) from 0000 UTC 10 September
154 2013 to 0000UTC 16 October 2013. Every simulation containing 10000 particles released at
155 the beginning over an altitude range of 3395 m a.s.l to 3995 m a.s.l and the model outputs
156 were recorded every 3-h. The output data of each simulation were combined together to make
157 the figure 1.

158 **2.5 PM_{2.5}, trace gases, BC, and meteorological measurements**

159 Thermo TEOM 1405 PM_{2.5} and PM₁₀ continually measure the particulate mass concentrations
160 in one-hour averages. Gaseous air pollutants were measured continuously from 1 September to 15
161 October, 2013: O₃ by a UV photometric analyzer (Teledyne Instruments, Model 400EU); SO₂ by a
162 pulsed UV fluorescence analyzer (M100EU), CO by a non-dispersive infrared analyzer (M300EU),
163 and NO and NO₂ by a commercial chemiluminescence analyzer (M200EU), with the
164 concentrations being recorded in five-minute averages. BC concentrations were measured by an
165 Aethalometer and were recorded in one hour averages. In addition, the non-refractory submicron
166 aerosol species including organics, sulfate, nitrate, ammonium, and chloride were measured in-situ
167 by an Aerodyne Aerosol Chemical Speciation Monitor (ACSM) (Du et al., 2015). Wind direction,
168 wind speed, relative humidity (RH), and temperature were measured and recorded in one hour
169 averages. The time-series meteorological data, shown in Figure S1, and the PM_{2.5} and gaseous
170 concentrations, were provided by the NSBAM.

171 The average CO mixing ratio is 44.78 ppb at the NSBAM, much lower than the 149 ppb at
172 Waliguan in the summer of 2006, that is the site of the observation station of the World
173 Meteorological Organization’s (WMO) Global Atmospheric Watch (GAW) (Xue et al., 2011). This
174 contrast shows that the NSBAM adequately represents background conditions in the expansive
175 grasslands of the northern TP. Time-series concentration variations of six pollutants (i.e., PM_{2.5},
176 BC, SO₂, NO_x, CO, and O₃) show that their highest concentrations occurred from 15 September to
177 25 September, 2013, and from 11 October to 15 October, 2013, (Figure 2). Therefore, we

178 considered these two periods as typical high-pollution events. Table 1 shows that five pollutants'
179 concentrations (i.e., PM_{2.5}, BC, SO₂, NO_x, and CO) were higher during these pollution events than
180 in the intervening cleaner period; O₃ concentration was close. When the combustion-tracing CO
181 and NO_x concentrations increase, O₃ mixing ratios generally decrease in the QTP due to
182 photochemical consumption (Xue et al., 2011). The primary BC concentrations during the two
183 pollution events were 17% and 81% higher than the intervening cleaner period, respectively
184 (Table 1). PM_{2.5} concentration at 17.06 µg/m³ at the NSBAM is slightly lower than the 21.5 µg/m³
185 in the cleaner Qinghai-lake area in the summer of 2010 (Li et al., 2013a). The air mass back
186 trajectories during the sampling period commonly came from the northwestern TP and crossed the
187 Qinghai-lake area into the northern TP (Figure 1). The air masses during the pollution events
188 adequately represented highly aged and processed long-range transported ambient aerosols in the
189 TP. Figure 2 further displays aerosol collection time under three different PM_{2.5} levels, e.g., PM_{2.5}
190 ≥ 30 µg/m³, PM_{2.5} between 10-30 µg/m³, PM_{2.5} < 10 µg/m³, which represent high pollution level,
191 medium pollution level, and clean pollution level.

192 **3. Results**

193 **3.1 Major fine aerosol particles and mixing states**

194 Based on elemental composition and morphology, aerosol particles were classified into six
195 major categories: mineral dust, K-Na-Cl, fly ash, secondary inorganic aerosol (SIA) containing
196 ammoniated sulfates and nitrates, organics, and soot (i.e., BC) (Figures 4-5). For example, mineral
197 dust particles normally display irregular shapes and fly ash particles are spherical, although they
198 both have similar compositions such as Si and Al. This detailed particle classification scheme is
199 described in our previous studies (Li et al., 2014b; Li et al., 2015). The nanosized metal particles
200 which have been frequently detected in ambient aerosols in East China (Li et al., 2013b; Li et al.,
201 2013c) were absent in the Qinghai-Tibet plateau. Mixing properties among the six types of
202 particles were characterized in detail. TEM observations indicate that SIA and organics coexisted
203 in individual fine particles and that organic carbon (OC) coated (e.g., Figures 4d and 5a) or
204 homogeneously mixed (e.g., Figure 6) with these SIA particles. In other words, OC occurred on
205 surfaces of the SIA particles. In addition, we found that many SIA-OC particles had visible
206 inclusions such as mineral dust, fly ash, OC, and soot particles. Identification of the refractory
207 inclusions in internally mixed particles enables one to trace particle sources and their history in the

208 aging air mass. Their mixing properties consist mostly of SIA-soot-OC (e.g., Figure 4c), SIA-fly
209 ash-soot (e.g., Figure 5d), SIA-fly ash-OC (visible) (e.g., Figure 5d), SIA-fly ash (e.g., Figure 5c),
210 SIA-mineral, SIA-visible OC (e.g., Figure 5a). Therefore, SIA and OC in aerosol particles in the
211 Qinghai-Tibet Plateau were the two most important influences of the mixing state of primary
212 particles.

213 **3.2 Size distribution of aerosol particles**

214 In this section, we describe the size distribution of individual particles with their diameters
215 from 40 nm to 1 μm in different pollution levels. 684 particles collected during clean periods show
216 a median diameter of 230 nm. Figure 7a shows that the size distribution of particles without
217 inclusions determines ambient particle size.

218 1214 particles during high pollution levels have a median diameter of 260 nm (Figure 7b).
219 Particles with inclusions and particles without inclusions have median diameters of 300 nm and
220 230 nm, respectively. Figure 7b shows particles with and without inclusions jointly determine the
221 particle size distribution during high pollution levels. We noticed that the size distribution of
222 inclusions in SIA displays a median diameter of 150 nm. A similar pattern of size distribution of
223 2355 particles occurred in medium pollution levels (Figure 7c). The median diameters of total
224 individual particles, particles with inclusions, particle without inclusions, and inclusions are 290
225 nm, 340 nm, 250 nm, and 150 nm, respectively. Therefore, the inclusions (e.g., mineral, fly ash,
226 soot, and spherical OC particles) significantly enhanced particle sizes in the background air once
227 they were internally mixed with sulfates.

228

229 **4. Discussion**

230 **4.1 Identification of the pollution events**

231 TEM observations show that individual particle types display large differences under three
232 different $\text{PM}_{2.5}$ levels: $\geq 30 \mu\text{g}/\text{m}^3$ (high pollution level), $10\text{-}30 \mu\text{g}/\text{m}^3$ (medium pollution level),
233 and $< 10 \mu\text{g}/\text{m}^3$ (clean pollution level) (Figure 3). Aerosol particles collected in clean periods
234 mainly contained SIA and OC. Figure 6 shows that individual SIA particles were commonly
235 coated by OC. Consistently, the ACSM measurement showed that SO_4^{2-} and OC were the main
236 components in PM_1 , accounting for 33-36% and 34-48% in mass at the sampling site, respectively
237 (Du et al., 2015). Figure 8 presents the composition of all the analyzed individual particles in the

238 three pollution levels. In the clean period, we found only a few anthropogenic particles such as fly
239 ash, soot, or their mixed particles with their contributions being less than 10% (Figure 8a).

240 The increase of KCl and soot particles is suggestive of an intense biomass burning event at the
241 background site (Li et al., 2003). In this study, abundant K-Na-Cl particles and soot-containing
242 particles (e.g., Figure 4) only occurred in pollution period 1 and period 2 which have been
243 indicated as biomass burning (Du et al., 2015). Because the K-Na-Cl particles associated with
244 OC occurred only in the short pollution periods and are smaller than typical sea-salt or soil
245 particles (mostly $>1\ \mu\text{m}$), it is unlikely that they originated from natural sources such as saline
246 Qinghai Lake and desert. Our field experimental investigations showed that a few farmers burned
247 cole flowers and highland barley during the autumn harvest season, which are main season crops
248 in the QTP. In addition, the burning of Yak dung for residential heating likely caused the high
249 $\text{PM}_{2.5}$ in 11-15 October (Du et al., 2015).

250 The distribution of different particle types in the medium pollution level is similar to the high
251 pollution level, except for the absence of K-Na-Cl particles. Figure 8c shows that a large amount
252 of fly ash-containing particles occurred in medium pollution level. Fly ash is generally considered
253 as a reliable fingerprint of coal combustion in residential cooking, power plants, and industrial
254 activities (Li and Shao, 2009). The fly ash-containing particles increase from 11.40% in the high
255 pollution level to 21.73% in the medium one, but soot-containing particles decrease from 38.40%
256 to 25.87%. This result indicates that coal combustion emissions in the QTP significantly affected
257 the background air quality. Compared to individual particles in polluted East China, absence of
258 nanometer metal particles in the QTP suggests that there are no large heavy metal-related
259 industrial emissions in the area under air mass back trajectories (Figure 1). The China Energy
260 Statistical Yearbook of 2013 shows coal combustion occurs in power plants (48.5%), heavy
261 industries (36.4%), and house cooking/heating in rural areas (8.6%) in Qinghai province,
262 particularly nearby the large cities such as Xi'ning (Wen et al., 2013). Although we didn't find any
263 K-Na-Cl particle in the samples under medium pollution level, 50% of SIA (OC coating) and
264 SIA-soot particles containing minor K (Figure 4c-d) frequently occurred in the samples. During
265 long-range transport, once coagulation and condensation of ammoniated sulfates and sulfuric acid
266 in biomass burning particles increase, K-rich particles may transform into sulfur-rich particles
267 with certain amounts of K (Li et al., 2014b). Therefore, SIA particles containing minor K suggest

268 that biomass burning emissions likely contributed to the QTP aerosols on a more or less constant
269 basis. A similar result has been obtained through the analysis of organic species in PM_{2.5} at
270 Qinghai-lake (Li et al., 2013a). Therefore, we conclude that emissions from biomass burning and
271 from coal combustion significantly contribute to the formation of anthropogenic fine particles in
272 the atmosphere over the QTP.

273 **4.2 Regional effects of biomass burning and industrial emissions**

274 The previous studies proved that trace gases such as SO₂, NO_x, and volatile organic
275 compounds (VOCs) from anthropogenic and natural sources had been transported long distances
276 in the QTP and were transformed into secondary aerosol particles (Xue et al., 2011;Li et al.,
277 2013a;Du et al., 2015;Xu et al., 2015). For example, *Du et al. (2015)* suggested that oxygenated
278 organic aerosols from anthropogenic sources and biomass burning transported over a long distance
279 to the sampling site in the QTP. Because of measurement limitations, there is no research about
280 refractory aerosol particles (e.g., mineral, fly ash, and soot) in fine particles and primary organic
281 particles. In contrast, TEM observations can adequately characterize these refractory particles
282 internally mixed with SIA based on their unique morphology and composition (Figures 4-5). We
283 identified abundant refractory particles at the three pollution levels at the regional background site.
284 Therefore, the nanosized refractory particles and trace gases from various anthropogenic sources
285 including biomass burning can together be transported long distances. The FLEXPART simulation
286 shows that these anthropogenic particles mainly originated from biomass burning between the
287 Qinghai lake and Menyuan county and heavy industries and coal-fired power plants in western
288 areas of Xining city (Figure 1).

289 **4.3 Mixing mechanisms of aged aerosol particles**

290 In this study, individual particle clearly containing more than two types of aerosol components
291 (e.g., mineral dust, K-Na-Cl, fly ash, SIA, organics, and soot) has been defined as aged particle.
292 More than 90% of particles at the background site were highly aged. SIA with OC coating were
293 the dominant particles and could determine the hygroscopic properties of the ambient aerosol
294 particles. OC coatings on inorganic particles can induce an early deliquescence of particle surface
295 compared to that of the pure inorganic compounds (Li et al., 2014a). Recently, Mikhailov et al.
296 (2015) found that the semi-solid state of the OC coating can lead to kinetic limitations of water
297 uptake and release during hydrate and dehydrate cycles in the background area. OC dominated in

298 fine particles, accounting for 43% of mass on average, followed by sulfate (28%) and nitrate (1%)
299 (Du et al., 2015). TEM observations further indicated that OC can heterogeneously and
300 homogeneously be mixed with all the fine SIA particles (Figures 6, 9-10). This finding is in
301 agreement with the study of new particle formation and growth events during the sampling period,
302 in which oxygenated organics significantly contributed into particle growth in the QTP (Du et al.,
303 2015). SIA with OC coating (i.e., particle without inclusions in Figure 7) shift to one smaller size
304 than the total individual particles. Gas condensation on the existing particles is an important
305 chemical process for formation of SIA with OC coating. Therefore, OC coating of the aged
306 aerosol particles is likely an important factor to determine particle hygroscopic growth and phase
307 transitions in the QTP.

308 Inclusions within SIA particles increase their size by 36-42% (Figure 7). The size distribution
309 of individual particles shows that particles without inclusions have a median size of 200 nm - 250
310 nm at the background site. Figure 7 shows that the number of particles with inclusions increases
311 substantially with diameters above 200 nm. In addition, Figures 9-10 show soot, fly ash, and
312 visible OC particles likely adhere to the surface of SIA particles, which is different from many
313 refractory particles embedded within SIA particles in East China (Li and Shao, 2009; Li et al.,
314 2011b; Li et al., 2014b). Therefore, the coagulation process between primary refractory particles
315 and SIA particles with diameters > 200 nm could be dominant in the atmosphere. The results are
316 different from the background aerosol particles in Siberia where these soot, fly ash and visible OC
317 particles are absent (Mikhailov et al., 2015). In particular, the mixing structure of soot on the
318 surface of SIA particles is different from the previous studies (Li et al., 2003; Adachi et al.,
319 2010; Li et al., 2015). Therefore, sulfates cannot act as the lens to enhance optical absorption of
320 soot particles before individual particles totally deliquesces in humid air (Ramanathan and
321 Carmichael, 2008). Light absorption of soot on surfaces of sulfate particles have 30% lower than
322 soot centered within sulfate particles (Adachi et al., 2010). We found that number of
323 soot-containing particles increase during the biomass burning periods (Figure 8b-c). Also, Figure 3
324 shows that the BC concentrations exceeded $1.0 \mu\text{g m}^{-3}$ during biomass burning periods which is
325 two times higher than the average value during the sampling period. As a result, large amounts of
326 soot particles from biomass burning in background atmosphere likely change atmospheric optical
327 absorption and modify optical feedback of ice/snow after their deposition in the QTP (Che et al.,

328 2011;Ming et al., 2012). The microstructure of soot particles can improve understanding of the
329 optical properties of fine aerosol particles and better evaluate their climate impacts using climate
330 models.

331 We also notice that a large number of particles without inclusions can occur with diameters >
332 300 nm, although the particle numbers decrease (Figure 7). TEM observations reveal distinct rims
333 on some larger particles, as the examples shown in Figures 5a, 5d, 9b, 10a. Our previous studies
334 showed that the cloud and fog residues on the substrate can display distinct rims (Kojima et al.,
335 2004;Li et al., 2011a;Li et al., 2011b). Therefore, these large particles with distinct rims probably
336 undergo complicated atmospheric transformation such as cloud/fog processing during their growth.
337 Briefly, our study indicates that aerosol particles in different size regimes have different
338 atmospheric chemical or physical processes in the background air over the QTP.

339 **4.4 Further considerations about fine particles over Qinghai-Tibetan plateau**

340 Emissions from coal combustion and biomass burning contribute fine particles into the
341 background air over the QTP. Because the complex aerosol particles from different anthropogenic
342 sources intruded into pristine background air, the suspended aerosols became highly aged.
343 Because of the sensitive feedback of climate in the TP, these aged aerosol particles in the plateau
344 become particularly interesting. Firstly, transport and sources of aerosol particles should be
345 evaluated, and, indeed, most studies in the TP have accomplished this (Cong et al., 2009a;Cong et
346 al., 2009b;Engling et al., 2011;Lu et al., 2012;Du et al., 2015;Xu et al., 2015). These studies all
347 suggested that long-range transport of fine particles from biomass burning and other
348 anthropogenic sources (cooking and vehicular emissions) often reach the TP. However, the
349 emissions of coal combustion from power plants or other industrial sources have a decided
350 regional influence. The statement has not been reported. Our studies provide new evidence that fly
351 ash particles serve as a reliable fingerprint of coal-combustion at the background site. Following
352 economic development in western China, coal combustion increases, chiefly for electrical power
353 generation and other industrial activities (Figure S2). Secondly, highly aged particles such as
354 ambient aerosols and CCN in the atmosphere and sediment in ice/snow can directly or indirectly
355 impact on climate in the TP (Cong et al., 2009b;You et al., 2010;Che et al., 2011;Lu et al.,
356 2012;Ming et al., 2012;He et al., 2014;Wang et al., 2015;Yang et al., 2015). At the background
357 sampling site the mean BC concentration was $0.54 \mu\text{g}/\text{m}^3$. Interestingly, we found that most fine

358 soot (BC) particles adhere to individual SIA (Figures 9-10) in the Qinghai plateau while many
359 soot particles were embedded within SIA in polluted areas of East China (Li and Shao, 2009; Li et
360 al., 2011b). The detailed physical properties (e.g., mixing structure and size) of soot in air and
361 ice/snow should be further studied in the TP, which can improve the current climate models.
362 Thirdly, fine aerosol particles in the TP mainly contain OC and sulfates with minor nitrates. The
363 result is largely different from fine particles with high nitrate in more polluted areas (Li et al.,
364 2013a; Du et al., 2015; Xu et al., 2015). Although regional transport from anthropogenic sources or
365 biomass burning significantly increase particle concentrations, mineral dust from surrounding
366 deserts and organics from plants are still dominant in the TP throughout the year (Zhang et al.,
367 2001b; Wang et al., 2010; Li et al., 2013a; Xu et al., 2014).

368

369 **5. Conclusions**

370 Time-series of six pollutants ($PM_{2.5}$, BC, SO_2 , NO_x , CO, and O_3) were obtained at a national
371 station of background atmospheric monitoring (NSBAM) on the top of Moshidaban Mountain in
372 the North QTP during 15 September – 15 October, 2013. The mean concentrations of $PM_{2.5}$, BC,
373 SO_2 , NO_x , CO, and O_3 were $17.06 \mu\text{g}/\text{m}^3$, $0.54 \mu\text{g}/\text{m}^3$, 1.27 ppb, 2.05 ppb, 44.78 ppb, and 50.00
374 ppb, respectively. TEM was employed to study individual fine particles with the diameter less
375 than $1 \mu\text{m}$ that were classified into six major particle types: mineral dust, K-Na-Cl, fly ash,
376 secondary inorganic aerosol (SIA) containing ammoniated sulfates and nitrates, organics, soot (i.e.,
377 BC). Individual fine particle types display large differences under three different $PM_{2.5}$ levels:
378 $PM_{2.5} \geq 30 \mu\text{g}/\text{m}^3$ (high pollution level), $10 \leq PM_{2.5} < 30 \mu\text{g}/\text{m}^3$ (medium pollution level), and $<$
379 $10 \mu\text{g}/\text{m}^3$ (clean period). Individual fine particles in clean periods mainly contained SIA and
380 organics. The presence of K-Na-Cl coated by organics and increased soot particles during high
381 pollution levels suggests an intense biomass burning event near the background site. Large
382 amounts of fly ash-containing particles occurred in medium pollution level. The fly ash-containing
383 particles increased from 11.40% at the medium pollution level to 21.73% at the high pollution
384 level, but soot-containing particles decreased from 38.40% to 25.87%. This result indicates that
385 coal combustion emissions in the QTP significantly affected the background air quality. In
386 addition, SIA particles containing minor K suggest that biomass burning emissions were a
387 constant contributor to aerosol particles in the QTP. We concluded that the emissions from

388 biomass burning and coal-used anthropogenic activities contribute anthropogenic particles into the
389 QTP atmosphere.

390 Aerosol particles containing SIA core and OC coating display smaller median size than the
391 total particles. Gas condensation on the particles is an important chemical process for their
392 formation. The number concentration of particles with inclusions increased markedly above 200
393 nm. TEM observations show that refractory aerosols (e.g., soot, fly ash, and visible organic
394 particles) likely adhere to the surface of SIA particles, suggesting physical coagulation could be
395 dominant in background air. These results notably improve our understanding of sources and
396 aging processes of long-range transported aerosols in the QTP. The transport of these aerosol
397 particles, as well as their, hygroscopic, and optical properties and atmospheric chemistry, require
398 further study in the TP.

399

400 **Author contribution:** W.J.L. and J.M.C. designed the research and wrote the paper; W.J.L. and
401 S.R.C. carried TEM and AFM experiments; Y.S.X., X.C.G., Y.L.Y., and X.Y.Y. conducted field
402 experiments; X.D.Z provided the online monitoring data; Y.S.X, J.M.C., Z.F.W., and W.X.W lead the
403 projects.

404 **Acknowledgements.** We appreciate Peter Hyde's comments and proofreading. We are grateful to
405 Yong Ren for processing FLEXPART data for figure 1. This work was supported by the National
406 Natural Science Foundation of China (41575116 and 41375133), Shandong Provincial Science
407 Fund for Distinguished Young Scholars, China (JQ201413), Young Scholars Program of
408 Shandong University (2015WLJH37), Taishan Scholars (ts20120522), Fundamental Research
409 Funds of Shandong University (2014QY001), and State Key Laboratory of Atmospheric
410 Boundary Layer Physics and Atmospheric Chemistry (LAPC-KF-2014-03).

411

412 **References**

- 413 Adachi, K., Chung, S. H., and Buseck, P. R.: Shapes of soot aerosol particles and implications for their
414 effects on climate, *J. Geophys. Res.*, 115, doi:10.1029/2009JD012868, 2010.
- 415 Cao, J., Tie, X., Xu, B., Zhao, Z., Zhu, C., Li, G., and Liu, S.: Measuring and modeling black carbon (BC)
416 contamination in the SE Tibetan Plateau, *J. Atmos. Chem.*, 67, 45-60, 2010.
- 417 Che, H., Wang, Y., and Sun, J.: Aerosol optical properties at Mt. Waliguan Observatory, China, *Atmos.*
418 *Environ.*, 45, 6004-6009, 2011.
- 419 Cong, Z., Kang, S., Dong, S., and Zhang, Y.: Individual particle analysis of atmospheric aerosols at Nam
420 Co, Tibetan Plateau, *Aerosol Air Qual. Res.*, 9, 323-331, 2009a.
- 421 Cong, Z., Kang, S., Smirnov, A., and Holben, B.: Aerosol optical properties at Nam Co, a remote site in
422 central Tibetan Plateau, *Atmos. Res.*, 92, 42-48, 2009b.
- 423 Cong, Z., Kawamura, K., Kang, S., and Fu, P.: Penetration of biomass-burning emissions from South Asia
424 through the Himalayas: new insights from atmospheric organic acids, *Sci. Rep.*, 5, DOI:
425 10.1038/srep09580, 2015.
- 426 Du, W., Sun, Y. L., Xu, Y. S., Jiang, Q., Wang, Q. Q., Yang, W., Wang, F., Bai, Z. P., Zhao, X. D., and Yang, Y.
427 C.: Chemical characterization of submicron aerosol and particle growth events at a national
428 background site (3295 m a.s.l.) in the Tibetan Plateau, *Atmos. Chem. Phys. Discuss.*, 15, 13515-13550,
429 2015.
- 430 Duo, B., Zhang, Y., Kong, L., Fu, H., Hu, Y., Chen, J., Li, L., and Qiong, A.: Individual particle analysis of
431 aerosols collected at Lhasa City in the Tibetan Plateau, *J. Environ. Sci.*, 29, 165-177, 2015.
- 432 Engling, G., Zhang, Y.-N., Chan, C.-Y., Sang, X.-F., Lin, M., Ho, K.-F., Li, Y.-S., Lin, C.-Y., and Lee, J. J.:
433 Characterization and sources of aerosol particles over the southeastern Tibetan Plateau during the
434 Southeast Asia biomass-burning season, *Tellus B*, 63, 117-128, 10.1111/j.1600-0889.2010.00512.x,
435 2011.
- 436 He, C., Li, Q., Liou, K.-N., Takano, Y., Gu, Y., Qi, L., Mao, Y., and Leung, L. R.: Black carbon radiative
437 forcing over the Tibetan Plateau, *Geophys. Res. Lett.*, 41, 2014GL062191, 2014.
- 438 Kojima, T., Buseck, P. R., Wilson, J. C., Reeves, J. M., and Mahoney, M. J.: Aerosol particles from tropical
439 convective systems: Cloud tops and cirrus anvils, *J. Geophys. Res.*, 109, 12201-12201, 2004.
- 440 Kopacz, M., Mauzerall, D. L., Wang, J., Leibensperger, E. M., Henze, D. K., and Singh, K.: Origin and
441 radiative forcing of black carbon transported to the Himalayas and Tibetan Plateau, *Atmos. Chem.*
442 *Phys.*, 11, 2837-2852, 2011.
- 443 Lau, K. M., Kim, M. K., and Kim, K. M.: Asian summer monsoon anomalies induced by aerosol direct
444 forcing: the role of the Tibetan Plateau, *Clim Dyn*, 26, 855-864, 2006.
- 445 Li, C., Kang, S., Zhang, Q., and Kaspari, S.: Major ionic composition of precipitation in the Nam Co
446 region, Central Tibetan Plateau, *Atmos. Res.*, 85, 351-360, 2007.
- 447 Li, J., Posfai, M., Hobbs, P. V., and Buseck, P. R.: Individual aerosol particles from biomass burning in
448 southern Africa: 2, Compositions and aging of inorganic particles, *J. Geophys. Res.*, 108,
449 doi:10.1029/2002JD002310, 2003.
- 450 Li, J. J., Wang, G. H., Wang, X. M., Cao, J. J., Sun, T., Cheng, C. L., Meng, J. J., Hu, T. F., and Liu, S. X.:
451 Abundance, composition and source of atmospheric PM 2.5 at a remote site in the Tibetan Plateau,
452 China, *Tellus B*, 65, 10.3402/tellusb.v65i0.20281, 2013a.
- 453 Li, W., Li, P., Sun, G., Zhou, S., Yuan, Q., and Wang, W.: Cloud residues and interstitial aerosols from
454 non-precipitating clouds over an industrial and urban area in northern China, *Atmos. Environ.*, 45,
455 2488-2495, 2011a.

456 Li, W., Wang, T., Zhou, S., Lee, S., Huang, Y., Gao, Y., and Wang, W.: Microscopic Observation of
457 Metal-Containing Particles from Chinese Continental Outflow Observed from a Non-Industrial Site,
458 *Environ. Sci. Technol.*, 47, 9124-9131, 2013b.

459 Li, W., Wang, Y., Collett, J. L., Chen, J., Zhang, X., Wang, Z., and Wang, W.: Microscopic Evaluation of
460 Trace Metals in Cloud Droplets in an Acid Precipitation Region, *Environ. Sci. Technol.*, 47, 4172-4180,
461 2013c.

462 Li, W., Chi, J., Shi, Z., Wang, X., Chen, B., Wang, Y., Li, T., Chen, J., Zhang, D., Wang, Z., Shi, C., Liu, L.,
463 and Wang, W.: Composition and hygroscopicity of aerosol particles at Mt. Lu in South China:
464 Implications for acid precipitation, *Atmos. Environ.*, 94, 626-636,
465 <http://dx.doi.org/10.1016/j.atmosenv.2014.06.003>, 2014a.

466 Li, W., Shao, L., Shi, Z., Chen, J., Yang, L., Yuan, Q., Yan, C., Zhang, X., Wang, Y., Sun, J., Zhang, Y., Shen,
467 X., Wang, Z., and Wang, W.: Mixing state and hygroscopicity of dust and haze particles before leaving
468 Asian continent, *J. Geophys. Res.*, 119, 1044-1059, 2014b.

469 Li, W., Shao, L., Zhang, D., Ro, C.-U., Hu, M., Bi, X., Geng, H., Matsuki, A., Niu, H., and Chen, J.: A review
470 of single aerosol particle studies in the atmosphere of East Asia: morphology, mixing state, source, and
471 heterogeneous reactions, *J. Clean. Prod.*, DOI:10.1016/j.jclepro.2015.1004.1050 (in press), 2015.

472 Li, W. J., and Shao, L. Y.: Transmission electron microscopy study of aerosol particles from the brown
473 hazes in northern China, *J. Geophys. Res.*, 114, doi:10.1029/2008JD011285, 2009.

474 Li, W. J., Zhou, S. Z., Wang, X. F., Xu, Z., Yuan, C., Yu, Y. C., Zhang, Q. Z., and Wang, W. X.: Integrated
475 evaluation of aerosols from regional brown hazes over northern China in winter: Concentrations,
476 sources, transformation, and mixing states, *J. Geophys. Res.*, 116, doi:10.1029/2010JD015099, 2011b.

477 Lu, Z., Streets, D. G., Zhang, Q., and Wang, S.: A novel back-trajectory analysis of the origin of black
478 carbon transported to the Himalayas and Tibetan Plateau during 1996-2010, *Geophys. Res. Lett.*, 39,
479 L01809, 10.1029/2011gl049903, 2012.

480 Mikhailov, E. F., Mironov, G. N., Pöhlker, C., Chi, X., Krüger, M. L., Shiraiwa, M., Förster, J. D., Pöschl, U.,
481 Vlasenko, S. S., Ryshkevich, T. I., Weigand, M., Kilcoyne, A. L. D., and Andreae, M. O.: Chemical
482 composition, microstructure, and hygroscopic properties of aerosol particles at the Zotino Tall Tower
483 Observatory (ZOTTO), Siberia, during a summer campaign, *Atmos. Chem. Phys.*, 15, 8847-8869,
484 10.5194/acp-15-8847-2015, 2015.

485 Ming, J., Du, Z., Xiao, C., Xu, X., and Zhang, D.: Darkening of the mid-Himalaya glaciers since 2000 and
486 the potential causes, *Environ. Res. Lett.*, 7, 014021, 10.1088/1748-9326/7/1/014021, 2012.

487 Posfai, M., and Buseck, P. R.: Nature and Climate Effects of Individual Tropospheric Aerosol Particles,
488 *Annu. Rev. Earth Pl. Sc.*, 38, 17-43, 2010.

489 Ramanathan, V., and Carmichael, G.: Global and regional climate changes due to black carbon, *Nature*
490 *Geosci.*, 1, 221-227, 2008.

491 Stohl, A., Hittenberger, M., and Wotawa, G.: Validation of the lagrangian particle dispersion model
492 FLEXPART against large-scale tracer experiment data, *Atmos. Environ.*, 32, 4245-4264,
493 [http://dx.doi.org/10.1016/S1352-2310\(98\)00184-8](http://dx.doi.org/10.1016/S1352-2310(98)00184-8), 1998.

494 Wang, Q. Y., Huang, R. J., Cao, J. J., Tie, X. X., Ni, H. Y., Zhou, Y. Q., Han, Y. M., Hu, T. F., Zhu, C. S., Feng,
495 T., Li, N., and Li, J. D.: Black carbon aerosol in winter northeastern Qinghai-Tibetan Plateau, China: the
496 effects from South Asia pollution, *Atmos. Chem. Phys. Discuss.*, 15, 14141-14169, 2015.

497 Wang, X., Huang, J., Zhang, R., Chen, B., and Bi, J.: Surface measurements of aerosol properties over
498 northwest China during ARM China 2008 deployment, *J. Geophys. Res.*, 115,
499 doi:10.1029/2009JD013467, 2010.

500 Wen, J., Meng, H., Wang, X., and coauthors: China Energy Statistical Yearbook, Department of Energy
501 Statistics, National Bureau of Statistics, People's Republic of China, Beijing, 1-355, 2013.

502 Xia, X., Zong, X., Cong, Z., Chen, H., Kang, S., and Wang, P.: Baseline continental aerosol over the
503 central Tibetan plateau and a case study of aerosol transport from South Asia, *Atmos. Environ.*, 45,
504 7370-7378, 2011.

505 Xu, B., Cao, J., Hansen, J., Yao, T., Joswita, D. R., Wang, N., Wu, G., Wang, M., Zhao, H., Yang, W., Liu, X.,
506 and He, J.: Black soot and the survival of Tibetan glaciers, *Proc. Natl. Acad. Sci. U.S.A.*, 106,
507 22114-22118, 2009.

508 Xu, J., Zhang, Q., Li, X., Ge, X., Xiao, C., Ren, J., and Qin, D.: Dissolved Organic Matter and Inorganic Ions
509 in a Central Himalayan Glacier—Insights into Chemical Composition and Atmospheric Sources, *Environ.*
510 *Sci. Technol.*, 47, 6181-6188, 2013.

511 Xu, J., Wang, Z., Yu, G., Qin, X., Ren, J., and Qin, D.: Characteristics of water soluble ionic species in fine
512 particles from a high altitude site on the northern boundary of Tibetan Plateau: Mixture of mineral
513 dust and anthropogenic aerosol, *Atmos. Res.*, 143, 43-56, 2014.

514 Xu, J. Z., Zhang, Q., Wang, Z. B., Yu, G. M., Ge, X. L., and Qin, X.: Chemical composition and size
515 distribution of summertime PM_{2.5} at a high altitude remote location in the northeast of the Qinghai–
516 Xizang (Tibet) Plateau: insights into aerosol sources and processing in free troposphere, *Atmos. Chem.*
517 *Phys.*, 15, 5069-5081, 2015.

518 Xue, L. K., Wang, T., Zhang, J. M., Zhang, X. C., Deliger, Poon, C. N., Ding, A. J., Zhou, X. H., Wu, W. S.,
519 Tang, J., Zhang, Q. Z., and Wang, W. X.: Source of surface ozone and reactive nitrogen speciation at
520 Mount Waliguan in western China: New insights from the 2006 summer study, *J. Geophys. Res.*, 116,
521 doi:10.1029/2010JD014735, 2011.

522 Yang, S., Xu, B., Cao, J., Zender, C. S., and Wang, M.: Climate effect of black carbon aerosol in a Tibetan
523 Plateau glacier, *Atmos. Environ.*, 111, 71-78, 2015.

524 You, Q., Kang, S., Flügel, W.-A., Sanchez-Lorenzo, A., Yan, Y., Huang, J., and Martin-Vide, J.: From
525 brightening to dimming in sunshine duration over the eastern and central Tibetan Plateau (1961–
526 2005), *Theor. Appl. Climatol.*, 101, 445-457, 2010.

527 Zhang, D., Iwasaka, Y., and Shi, G.: Soot particles and their impacts on the mass cycle in the Tibetan
528 atmosphere, *Atmos. Environ.*, 35, 5883-5894, 2001a.

529 Zhang, X. Y., Arimoto, R., Cao, J. J., An, Z. S., and Wang, D.: Atmospheric dust aerosol over the Tibetan
530 Plateau, *J. Geophys. Res.*, 106, 18471-18476, 2001b.

531 Zhao, Z., Cao, J., Shen, Z., Xu, B., Zhu, C., Chen, L. W. A., Su, X., Liu, S., Han, Y., Wang, G., and Ho, K.:
532 Aerosol particles at a high-altitude site on the Southeast Tibetan Plateau, China: Implications for
533 pollution transport from South Asia, *J. Geophys. Res.*, 118, 11,360-311,375, 2013.

534 Zheng, W., Yao, T., Joswiak, D. R., Xu, B., Wang, N., and Zhao, H.: Major ions composition records from
535 a shallow ice core on Mt. Tanggula in the central Qinghai-Tibetan Plateau, *Atmos. Res.*, 97, 70-79,
536 2010.

537

538

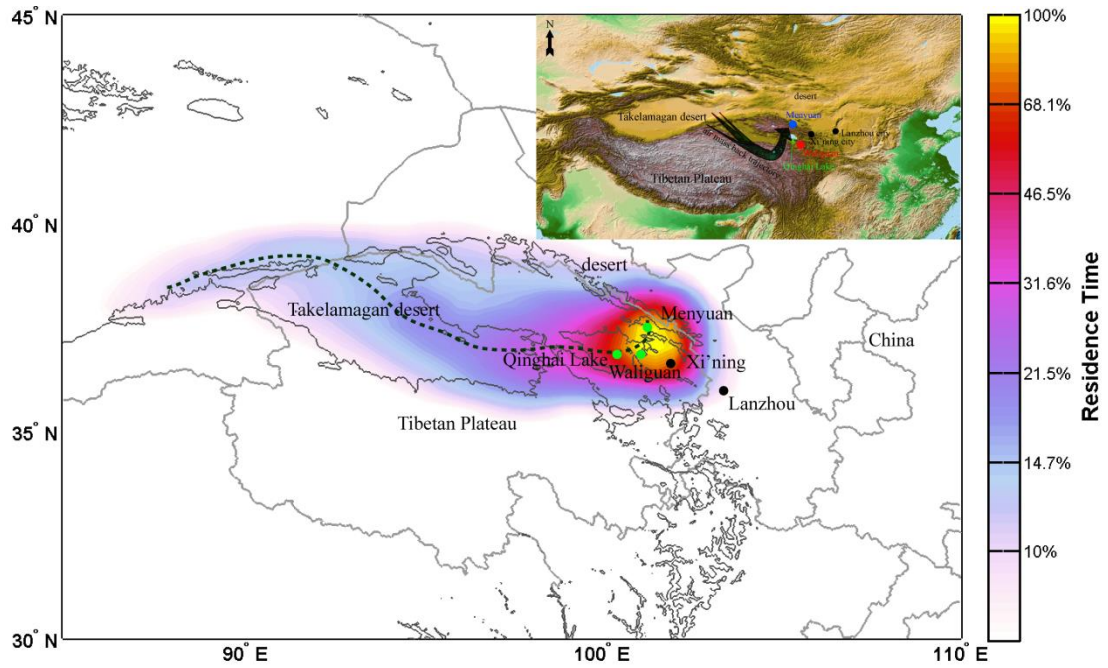


Figure 1 FLEXPART retrorplume simulations during 10 September-15 October. Topographical map showing the sampling location and surrounding regions in the Tibetan Plateau. Xi'ning is the caption city of Qinghai province. Menyuan represents sampling site. The black line shows the major back trajectories of air mass during 10 September - 15 October, 2013 based on the spatial distribution of the air mass. The main air mass mainly passed through rural areas, grasslands, and desert.

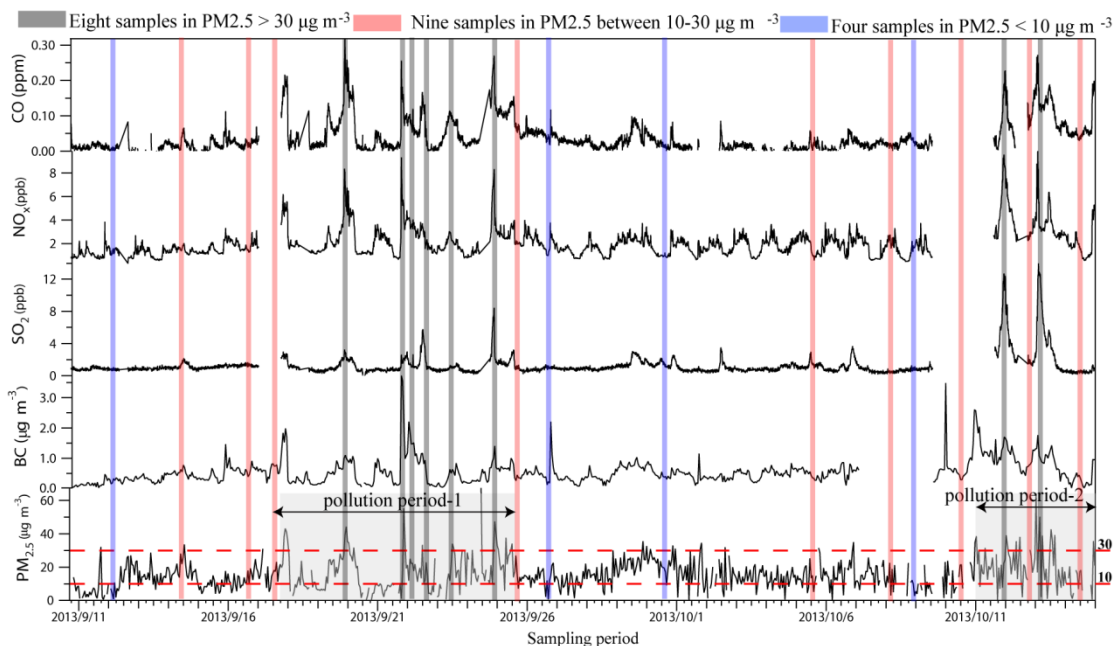


Figure 2 Time-series concentration of air pollutants (i.e., CO, NO_x, SO₂, BC, and PM_{2.5}) during 11 September – 15 October, 2013. The sampling time was marked by grey column (PM_{2.5} ≥ 30 µg/m³), pink column (PM_{2.5} between 10-30 µg/m³), blue column (PM_{2.5} < 10 µg/m³).

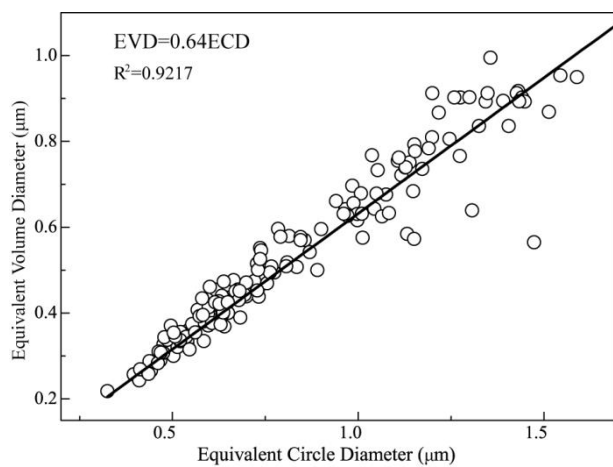


Figure 3 Correction of equivalent circle diameters (ECD) vs equivalent volume diameter (EVD) of 194 aerosol particles.

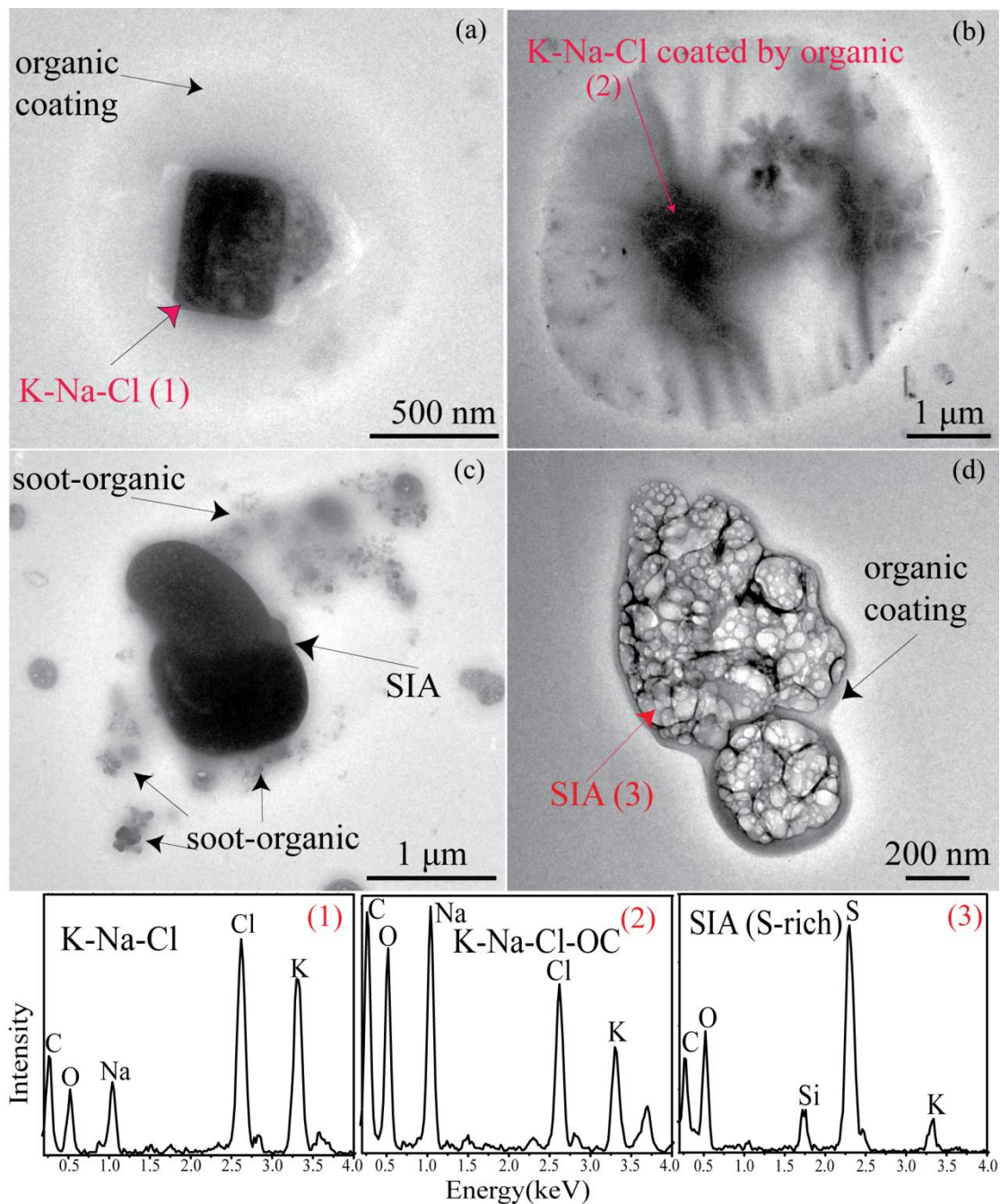


Figure 4 TEM images of (a-b) K-Na-Cl particle with organic coating on 22 September and 13 October. (c) SIA-soot with organic coating on 22 September. (d) SIA with organic coating on 11 October. EDS spectra shows elemental compositions of each particle type in each TEM image.

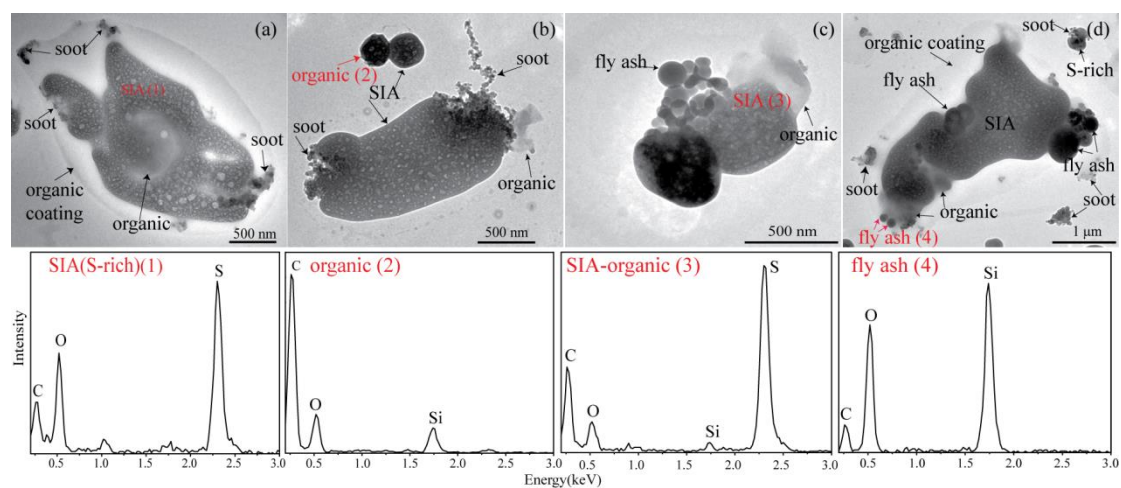


Figure 5 TEM images of (a) SIA-soot-OC (visible) with organic coating on 16 September. (b) SIA-soot-OC on 14 September. (c) SIA-fly ash-OC on 5 October. (d) SIA-fly ash-soot-OC (visible) with organic coating on 16 September. EDS spectra shows elemental composition of each particle type in each TEM image.

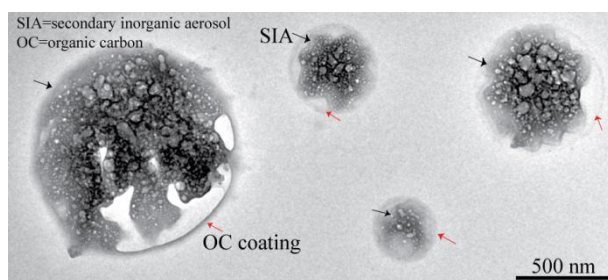


Figure 6 TEM image of individual particles collected in clean period with $PM_{2.5}$ mass concentration less than $10 \mu\text{g}/\text{m}^3$. SIA particles tend to homogeneously mix with organics.

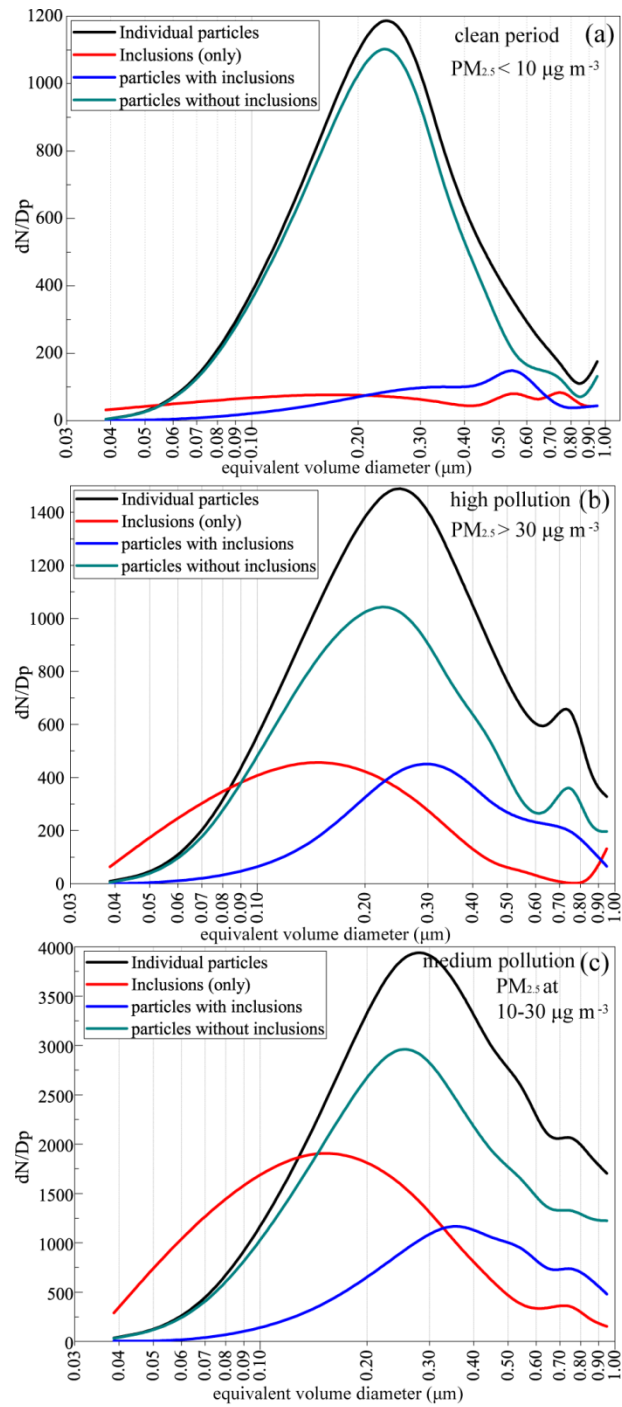


Figure 7 Size distributions of individual particles, inclusions, particles with inclusions, and particles without inclusions. (a) Clean periods under PM_{2.5} at 10 μg/m³. (b) The high pollution level under PM_{2.5} larger than 30 μg/m³. (c) The medium pollution level under PM_{2.5} among 10 μg/m³ - 30 μg/m³.

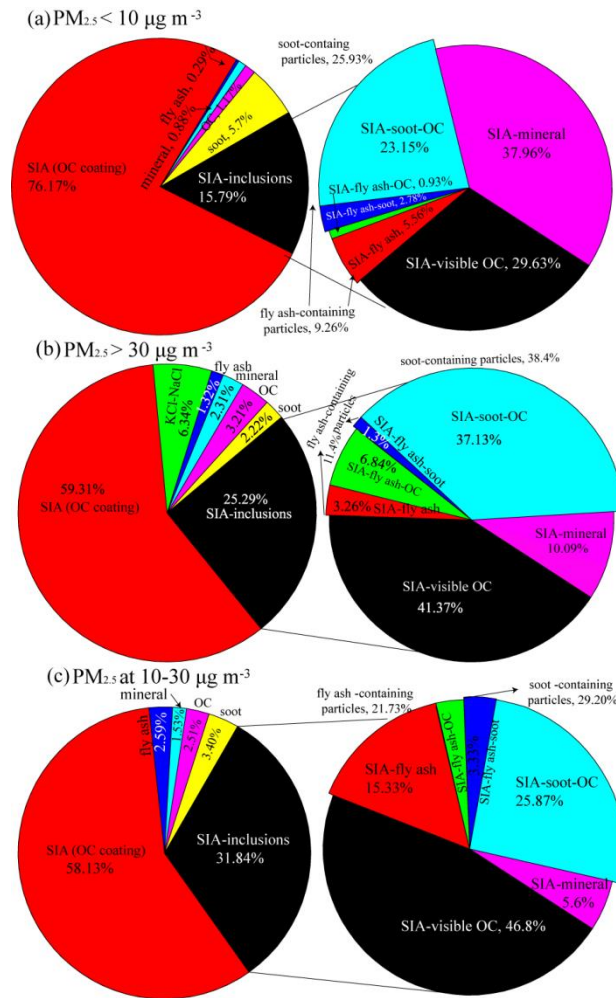


Figure 8 Identification of the pollution events based on individual particle analysis (a) 684 individual particles and 108 SIA-inclusion particles. (b) 1214 individual particles and 307 SIA-inclusion particles. Eight samples were collected in $PM_{2.5}$ larger than $30 \mu g m^{-3}$ induced by biomass burning emission. (c) 2355 individual particles and 750 SIA-inclusion particles. Nine samples were collected in $PM_{2.5}$ at the range of $10-30 \mu g m^{-3}$ induced by biomass burning and industrial emissions. Four samples were collected in $PM_{2.5}$ smaller than $10 \mu g m^{-3}$ which indicates clean period.

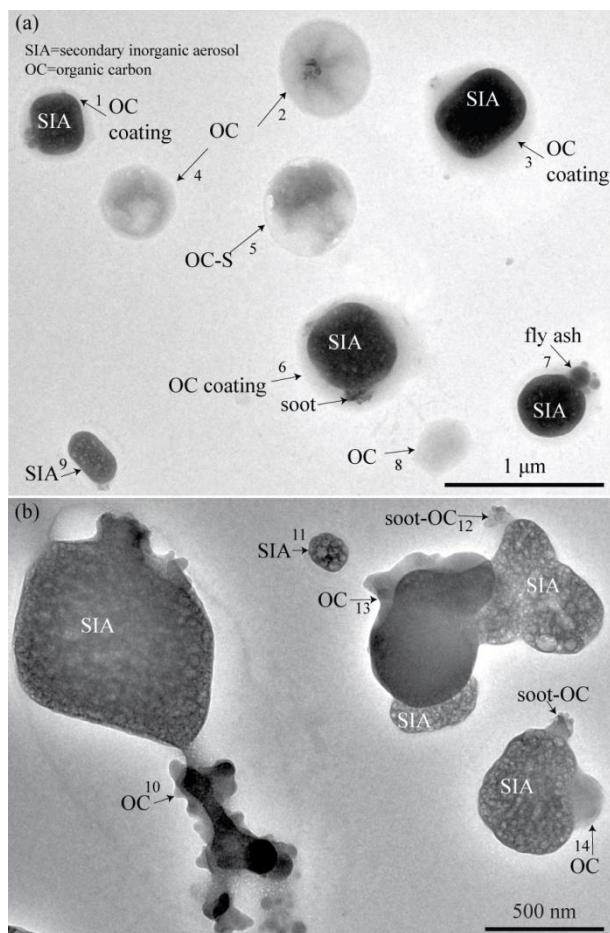


Figure 9 Individual particles during biomass burning periods with $PM_{2.5}$ mass concentration larger than $30 \mu\text{g}/\text{m}^3$. (a) OC and SIA-soot-(OC coating) particles on 12 October. (b) SIA-soot-(visible OC) on 19 October. OC in particles 1, 3, 6, 10, 13, 14 are heterogeneously mixed with SIA particles and particles 2, 4, 5, 8 homogeneously mixed with minor SIA.

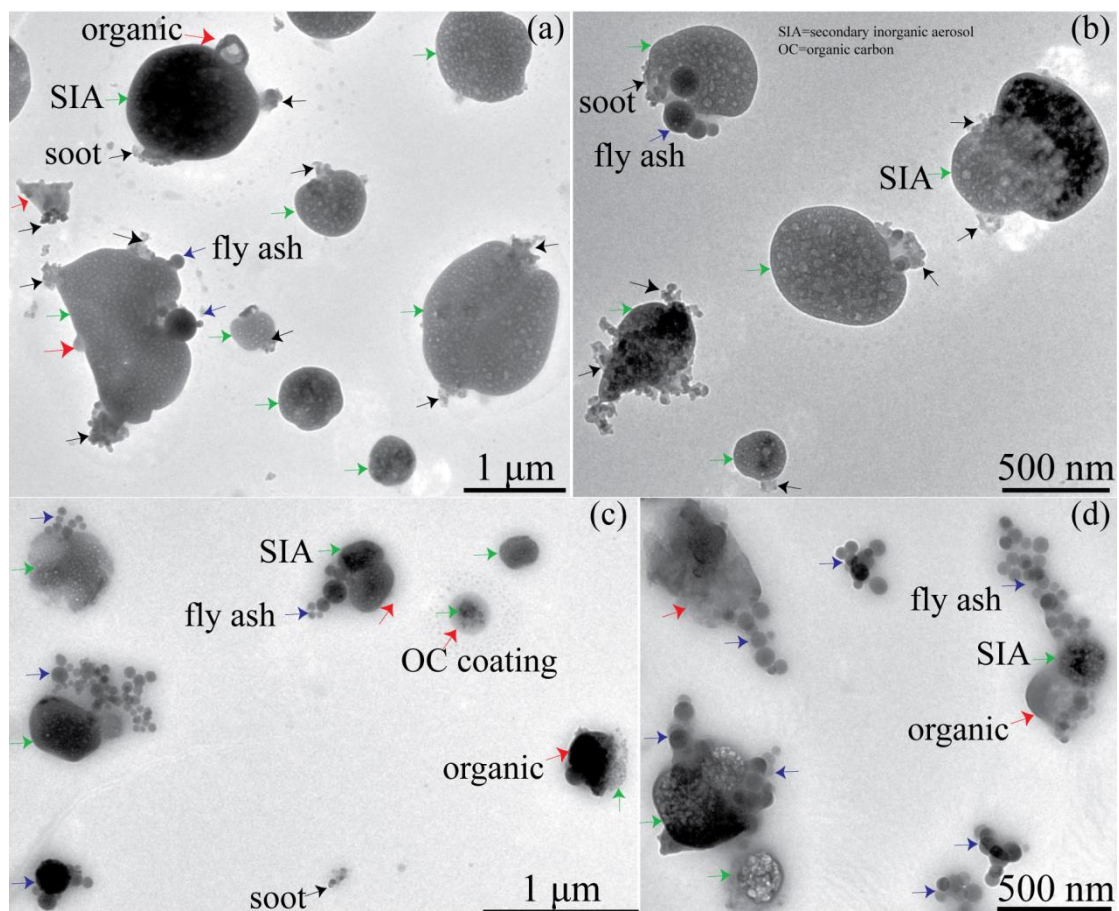


Figure 10 Individual particles collected under $PM_{2.5}$ mass concentration among $10\text{-}30\ \mu\text{g}/\text{m}^3$. (a) Mixture of SIA and soot, fly ash particles collected on 14 September. (b) Mixture of SIA and soot, fly ash particles collected on 18 September. (c) Mixture of SIA and fly ash, soot, organics collected on 29 September. (c) Mixing of SIA and fly ash, soot, organics collected on 10 October. Organics are heterogeneously mixed with SIA.

Table 1 Concentrations of six air pollutants during the sampling period, two pollution periods, and clean period

Pollutants	All data		polluted period-1		polluted period-2		other period	
	mean \pm SD	n	mean \pm SD	n	mean \pm SD	n	mean \pm SD	n
	Max, Min		Max, Min		Max, Min		Max, Min	
PM _{2.5}	17.06 \pm 1.39	715	17.6 \pm 1.46	152	24.45 \pm 15.12	99	15.32 \pm 0.41	464
	68.70, 0.20		59.10, 0.20		68.70, 0.30		62.80, 0.20	
BC	0.54 \pm 0.42	805	0.55 \pm 0.52	176	0.85 \pm 0.50	119	0.47 \pm 0.40	510
	3.73, 0.02		3.73, 0.04		2.04, 0.02		3.73, 0.03	
SO ₂	1.27 \pm 1.34	8822	1.2 \pm 0.99	1981	2.73 \pm 3.09	1063	1.03 \pm 0.65	5778
	13.93, 0.02		8.43, 0.20		13.93, 1.41		8.43, 0.02	
NO _x	2.05 \pm 1.96	8842	2.37 \pm 1.33	2001	3.41 \pm 1.70	1063	1.69 \pm 0.97	5778
	9.86, 0.31		9.33, 0.65		9.59, 0.55		9.33, 0.31	
CO	44.78 \pm 48.03	7822	63.45 \pm 55.59	1939	104.23 \pm 54.69	1030	24.68 \pm 39.91	4853
	318.00, 0.20		318.00, 0.20		272.40, 0.60		318.00, 0.20	
O ₃	50 \pm 7.86	8817	47.87 \pm 7.70	2000	49.01 \pm 10.00	1039	50.53 \pm 7.56	5778
	98.63, 20.43		67.70, 26.66		98.63, 20.43		96.77, 26.66	

All data period: 10 Sept.-15 Oct. 2013; Polluted period-1: 18 Sept.-25 Sept. 2013; Polluted period-2: 11 Oct.-15 Oct. 2013